42061

GEOPHYSICS, VOL. 72, NO. 5 (SEPTEMBER-OCTOBER 2007); P. E149–E158, 6 FIGS., 1 TABLE.
10.1190/1.2749571

Dynamic permeability of porous rocks and its seismic signatures

Tobias M. Müller[1], Gracjan Lambert[2], and Boris Gurevich[3]

ABSTRACT

In inhomogeneous porous media, the mechanism of wave-induced fluid flow causes significant attenuation and dispersion of seismic waves. In connection with this phenomenon, we study the impact of spatial permeability fluctuations on the dynamic behavior of porous materials. This heterogeneous permeability distribution further complicates the ongoing efforts to extract flow permeability from seismic data. Based on the method of statistical smoothing applied to Biot's equations of poroelasticity, we derive models for the dynamic-equivalent permeability in 1D and 3D randomly inhomogeneous media. The low-frequency limit of this permeability corresponds to the flow permeability governing fluid flow in porous media. We incorporate the dynamic-equivalent permeability model into the expressions for attenuation and dispersion of P-waves, also obtained by the method of smoothing. The resulting attenuation and dispersion model is confirmed by numerical computations in randomly layered poroelastic structures. The results suggest that the effect of wave-induced fluid flow can be observed in a broader frequency range than previously thought. The peak attenuation shifts along the frequency axis depending on the strength of the permeability fluctuations. We conclude that estimation of flow permeability from seismic attenuation is only possible if permeability fluctuations are properly accounted for.

INTRODUCTION

Permeability variations in sedimentary rocks are important for predicting fluid flow through these porous structures. Over the years, numerous papers have been published discussing varying methodologies for computing an effective flow permeability for heterogeneous structures based on Darcy's law (e.g., Beran, 1968; Hristopulos and Christakos, 1997; Keller, 2001). It has been shown that the effective flow permeability depends on the observation scale: both positive scale effect (larger permeability for larger observation scale) and negative scale effect are reported (Schulze-Makuch et al., 1999; Bernabé et al., 2003). Because permeability is a major control of fluid flow, to understand the dependence of seismic amplitudes on permeability would be enormously important for the oil industry as pointed out by Pride et al., 2003.

In porous media with mesoscale inhomogeneities of the elastic moduli, the effect of wave-induced fluid flow causes significant attenuation and dispersion of seismic waves (Pride et al., 2004; Müller and Gurevich, 2005b). Mesoscale refers to a length scale which is much larger than typical scales of the pore space and which is much smaller than the wavelength of the seismic wave. Therefore, accurate measurements of frequency-dependent attenuation have the potential to provide estimates of the flow permeability using seismic data. However, existing models of wave-induced fluid flow in randomly inhomogeneous porous media are often limited to a small contrast in all poroelastic constants (porosity, permeability, density, elastic moduli, etc.). Under this condition, the effect of permeability fluctuations on seismic velocity and attenuation is negligible (compared to a similar contrast in porosity or drained bulk modulus), and thus, a uniform permeability may be assumed (Müller and Gurevich, 2005a). Numerical tests in 1D showed that these models work for relative contrasts of at least 30% (Gurevich et al., 1997; Gelinsky et al., 1998; Pride et al., 2002; Carcione and Picotti, 2006). Spatial fluctuations of porosity, solid and fluid densities, or elastic moduli seldom exceed such contrast. On the other hand, permeability can vary by orders of magnitude over short distances. Therefore, the effect of spatial variations of permeability on wave-induced flow must be taken into consideration.

Berryman (1986, 1988) raised concern about the correct permeability average in the context of the Biot global flow attenuation. Shapiro and Müller (1999) first noticed the discrepancy between the searched-for flow permeability κ and the permeability controlling seismic attenuation related to interlayer flow in randomly layered

Manuscript received by the Editor January 22, 2007; published online July 10, 2007.
[1]University of Karlsruhe, Geophysical Institute, Karlsruhe, Germany. E-mail: tobias.mueller@gpi.uni-karlsruhe.de.
[2]Formerly Curtin University of Technology, Department of Exploration Geophysics, Perth, Western Australia; presently Total E&P, UK Limited, Geoscience Research Centre, Aberdeen, United Kingdom. E-mail: gracjan.lambert@total.com.
[3]Curtin University of Technology, Department of Exploration Geophysics, Perth, Western Australia and CSIRO Petroleum, Bentley, Western Australia. E-mail: boris.gurevich@geophy.curtin.edu.au.

porous media. Through comparison of theoretical and numerical attenuation estimates, they demonstrate that the exact flow permeability $\langle 1/\kappa \rangle^{-1}$, i.e., the harmonic average over the layer permeabilities, is unable to account for the attenuation observed in the numerical results. To obtain the correct permeability, they proposed to use the arithmetic average over the layer permeabilities, i.e., $\langle \kappa \rangle$. This arithmetically averaged permeability is referred to as the seismic permeability because it controls approximately the seismic attenuation behavior. Though this approach is somewhat heuristic, it shows that the influence of permeability fluctuations on seismic attenuation has important implications. Any attempt to estimate the flow permeability from seismic signatures will be biased when permeability fluctuations are not properly accounted for.

In this paper, we attempt to determine the impact of permeability fluctuations on the dynamic behavior of porous media caused by wave-induced flow only using a theoretical approach. Based on the method of statistical smoothing for Biot's equations of poroelasticity (Müller and Gurevich, 2005a, 2006), we derive a dispersion equation for the slow P-wavenumber in the presence of mesoscopic permeability fluctuations. From this result, we identify an effective permeability which exhibits dynamic behavior in the seismic frequency band. This is different from the model of Johnson et al. (1987), which predicts frequency-dependent permeability related to inertial effects at frequencies of the order of Biot's critical frequency (Biot, 1962):

$$\omega_c = \frac{\phi\eta}{\kappa\rho_f}, \tag{1}$$

where ϕ is the porosity, η is the fluid viscosity, and ρ_f is the fluid density. The latter mechanism produces practically no frequency dependency for typical reservoir rocks at seismic frequencies.

To have a clear separation between these mechanisms we assume throughout the paper that

$$\omega \ll \omega_c. \tag{2}$$

We also note that all wave attenuation mechanisms other than wave-induced flow, which might be active in the frequency range (equation 2), are not considered in the following. In a second step, we incorporate the dynamic-equivalent permeability model into the expressions for the effective fast P-wavenumber (according to Müller and Gurevich, 2005b) from which attenuation and velocity dispersion are computed. Despite the fact that these results are based on weak-fluctuation theory, it is shown that the essential effect of permeability fluctuations — namely, a frequency shift of the wave-induced attenuation — can be modeled. For 1D random media, the results can be extended to model the impact of stronger permeability fluctuations. The predicted attenuation and velocity dispersion curves for randomly layered media are also compared to numerical results.

DISPERSION RELATION FOR BIOT'S SLOW WAVE AND THE DYNAMIC-EQUIVALENT PERMEABILITY

The slow P-wave (Biot's second compressional wave, Biot 1956) in homogeneous porous media is a highly dissipative wave mode. In an inhomogeneous porous medium, the effective slow P-wave will be additionally attenuated and dispersed due to interaction with inhomogeneities. Within the assumptions of the first-order statistical smoothing applied to the low-frequency version of Biot's equations of poroelasticity (Biot, 1962), the effective slow P-wavenumber k_2^* in 3D statistically isotropic random media obeys a dispersion relation of the form (Müller and Gurevich, 2006; see also Appendix A),

$$k_2^{*2} = k_2^2\left[1 + \Delta_S\xi(\omega)\right], \tag{3}$$

where ξ is a frequency-dependent function,

$$\xi(\omega) = 1 + k_2^2\int_0^\infty rB(r)\exp(ik_2r)dr, \tag{4}$$

and Δ_S is a dimensionless coefficient containing the fluctuations of the poroelastic parameters:

$$\Delta_S = \left\langle\left(\frac{\alpha^2M}{P_d}\varepsilon_\alpha - \varepsilon_{K_f} + \varepsilon_\phi\right)^2\right\rangle + \frac{\sigma_{pp}^2}{3}. \tag{5}$$

Finally, in equation 3, k_2 denotes the wavenumber of a slow P-wave propagating in a constant background medium (no fluctuations).

$$k_2 = \sqrt{i\omega\eta/(\kappa_0N)}, \tag{6}$$

where κ_0 is the permeability in the background medium with fluid viscosity η and with $N = MP_d/H$ being a combination of poroelastic moduli specified as follows: H is the undrained low-frequency P-wave modulus given by Gassmann's equation $H = P_d + \alpha^2M$, M is the pore-space modulus of the drained frame defined as $M = [(\alpha - \phi)/K_g + \phi/K_f]^{-1}$, $P_d = K_d + 4/3G$ is the P-wave modulus of the drained frame, and $\alpha = 1 - K_d/K_g$ is the Biot-Willis coefficient. The terms K_g, K_d, and K_f denote the bulk moduli of the solid phase, the drained frame, and the fluid phase, respectfully, whereas G denotes the porous material shear modulus. In equations 4 and 5, the following statistical notations are introduced: $B(r)$ is the normalized autocorrelation function such that $B_{XY} = \sigma_{XY}^2B(r)$ with $B(0) = 1$; and $B_{XX}(\delta r) = \langle\varepsilon_X(r + \delta r)\varepsilon_X(r)\rangle$, where the angular brackets denote ensemble averaging. The relative fluctuations of the poroelastic parameters are denoted as ε_X; they have zero mean, $\langle\varepsilon_X\rangle = 0$, and variance $\langle\varepsilon_X^2\rangle = \sigma_{XX}^2$. Note that the permeability fluctuations enter in equation 5 through the variance of the reciprocal permeability ($p = 1/\kappa_0$) fluctuations. In 1D random media, equation 3 can be used together with

$$\xi^{(1D)}(\omega) = 1 + ik_2\int_0^\infty B(r)\exp(ik_2r)dr \tag{7}$$

and

$$\Delta_S^{(1D)} = \left\langle\left(\frac{\alpha^2M}{P_d}\varepsilon_\alpha - \varepsilon_{K_f} + \varepsilon_\phi\right)^2\right\rangle + \sigma_{pp}^2. \tag{8}$$

Despite the fact that dispersion relation 3 is only valid for small fluctuations in the rock properties, it reveals the essential physics as discussed in the following.

The result for the effective slow P-wave number (equation 3) allows us to derive a model for an effective (dynamic-equivalent) permeability for both 3D and 1D random media. If we assume that k_2^* is of the form $k_2^* = \sqrt{i\omega\eta/\kappa^*N}$ involving an effective permeability κ^*, the latter equation can be solved for κ^*, and equation 3 can be substituted for k_2^*. Taking the real part (the imaginary part of κ^* is not relevant in the sequel), we obtain, for 3D random media in the weak-fluctuation approximation,

$$\frac{\kappa^{*(3D)}}{\kappa_0} = 1 - \frac{\sigma_{pp}^2}{3} + \frac{2}{3}\sigma_{pp}^2 k_{2R}^2 \int_0^\infty rB(r) \times \exp(-k_{2R}r)\sin(k_{2R}r)dr, \quad (9)$$

where k_{2R} denotes the real part of k_2 (equation 6). Analogously, for 1D random media, we obtain from equations 3, 7, and 8,

$$\frac{\kappa^{*(1D)}}{\kappa_0} = 1 - \sigma_{pp}^2 + \sqrt{2}\sigma_{pp}^2 k_{2R} \int_0^\infty B(r)\exp(-k_{2R}r) \times \sin(k_{2R}r + \pi/4)dr. \quad (10)$$

The frequency dependence of these effective permeabilities is illustrated in Figure 1. It can be observed that the permeability dispersion effect is more pronounced in 1D than in 3D random media. The integrals in equations 9 and 10 involving the spatial correlation function show the nonlocal character of the effective permeability. This dispersion is the physical consequence of the existence of a characteristic length scale in the spatial permeability fluctuations.

In the low-frequency limit, the integral terms in equations 9 and 10 vanish such that

$$\kappa^{*(3D)}(\omega \to 0) \approx \kappa_0\left(1 - \frac{\sigma_{\kappa\kappa}^2}{3}\right) \quad (11)$$

and

$$\kappa^{*(1D)}(\omega \to 0) \approx \kappa_0(1 - \sigma_{\kappa\kappa}^2). \quad (12)$$

Note that equation 12 corresponds to the harmonically averaged permeability $\langle 1/\kappa\rangle^{-1}$, provided that $\sigma_{\kappa\kappa}^2 < 1$. Therefore, the low-frequency limit of the effective permeability corresponds to the searched-for flow permeability. It is interesting to note that the same low-frequency limit, equation 11, is also obtained by Keller (2001), using the method of smoothing applied to Darcy's law. Moreover, it is well known that the factor 1/3 in equation 11 reflects the assumption of statistical isotropy in 3D random media and is typical for effective permeability analysis in weakly inhomogeneous structures (Beran, 1968). In the high-frequency limit, only the behavior of the correlation function at small argument is of importance. All correlation-function models that have power-series expansion of the form $B(r/a) = 1 - r/a + O(r^2/a^2)$ (where a is the correlation length), produce, after substitution of $B(r/a) \approx 1 - r/a$ into equations 9 and 10 and integration,

$$\kappa^{*(3D)}(\omega \to \infty) = \kappa^{*(1D)}(\omega \to \infty) = \kappa_0, \quad (13)$$

i.e., the arithmetic average of the permeability values. Further properties of this frequency-dependent, effective permeability are discussed in Müller and Gurevich (2006).

For 1D random media, the result for the effective permeability can be improved using the fact that the low- and high-frequency results (equations 12 and 13) correspond to the exact bounds (e.g., Hristopulos and Christakos, 1997). If we assume that the frequency-dependent part of equation 10 interpolates correctly between the harmonic and arithmetic average, $\langle\frac{1}{\kappa}\rangle^{-1}$ and $\langle\kappa\rangle$, for any given contrast, equation 10 can be rescaled into

$$\frac{\kappa^{*(1D)}}{\kappa_0} = \left\langle\frac{1}{\kappa}\right\rangle^{-1}\langle\kappa\rangle^{-1} + \sigma_R^2\sqrt{2}k_{2R}\int_0^\infty B(r) \times \exp(-k_{2R}r)\sin(k_{2R}r + \pi/4)dr, \quad (14)$$

where the "contrast" σ_R^2 is now expressed as the normalized difference of the arithmetic and harmonic average:

$$\sigma_R^2 = 1 - \left[\left\langle\frac{1}{\kappa}\right\rangle\langle\kappa\rangle\right]^{-1}. \quad (15)$$

For strong permeability fluctuations, we expect $\langle\kappa\rangle \gg \langle\frac{1}{\kappa}\rangle^{-1}$ such that $\sigma_R^2 \to 1$. We note that the rescaling operation (i.e., the multiplication with the normalized difference σ_R^2) used to obtain equation 14 is not based on a rigorous mathematical formalism but is guided by the exact physical results available in space dimension one. In other words, our *ansatz* is to use the frequency dependence of the permeability determined in a weak-fluctuation approximation as an interpolation function between the exact bounds. The resulting effective permeability (equation 14) is no longer restricted to weak fluctuations.

In summary, in the presence of mesoscopic heterogeneities (in particular, permeability fluctuations), the permeability becomes a frequency-dependent quantity. Dispersion relations for this quantity can be derived from the dispersion relation for Biot's slow wave involving the second-order statistics of the fluid transport and poroelastic moduli fluctuations. In the next section, we use this permeability model to quantify the effect of permeability fluctuations on the signatures of seismic waves.

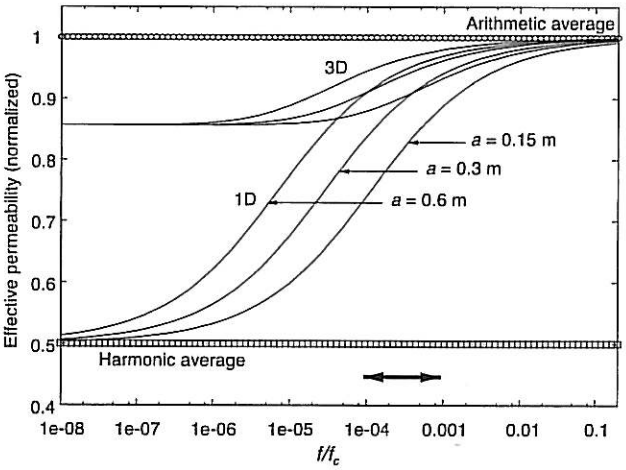

Figure 1. Frequency dependence of the effective permeability for 1D and 3D random media for varying correlation lengths of the permeability fluctuations (the correlation lengths are from left to right: a = 0.6 m, 0.3 m, 0.15 m). The frequency is normalized by the critical Biot frequency f_c = 108 kHz; the effective permeability is normalized by the arithmetic average of the permeability fluctuations $\langle\kappa\rangle = \kappa_0$. The effect of permeability dispersion is more pronounced in 1D than in 3D random media. The thick arrow indicates the surface seismic frequency range, 10 to 100 Hz. The lower bound is the harmonic average of permeability fluctuations and is an exact result for 1D random media (depicted by squares), whereas the upper bound (depicted by circles) is given by the arithmetic average of permeability fluctuations and is exact for all space dimensions (see also equation 13).

SEISMIC SIGNATURES OF PERMEABILITY FLUCTUATIONS

The physics of wave-induced flow can be interpreted as conversion scattering at heterogeneities from the fast P-wave into the diffusive slow P-wave mode (Gurevich and Lopatnikov, 1995; Gelinsky and Shapiro, 1997; Gelinsky et al., 1998). The resulting attenuation of the fast P-wave is, therefore, dependent on the characteristics of the slow P-wave described by one or another approximation. At sufficiently low frequencies and higher concentrations of heterogeneities, the slow P-wave will interact with these heterogeneities (in particular, with spatial permeability fluctuations). To our knowledge, these slow P-wave scattering effects are neglected in all theoretical descriptions of wave-induced flow in random porous media. In light of the results of the previous section, this also indicates that fluctuations in the transport properties are not properly accounted for. A natural way to incorporate the slow P-wave scattering effects and, hence, the dependence on transport property fluctuations into theories of wave-induced flow is to replace the slow P-wavenumber (equation 6) by its effective value derived in the previous section (equation 3). This strategy can be applied in 1D as well as in 3D media and will be pursued in the following.

Weak permeability fluctuations in 3D random media

The method of statistical smoothing applied to Biot's equation of poroelasticity yields an effective fast P-wavenumber k_1^* that accounts for the effect of wave-induced fluid flow (Müller and Gurevich, 2005b, their equation 1):

$$k_1^* = k_1\left(1 + \Delta_2 + \Delta_1 k_2^2 \int_0^\infty rB(r)\exp(ik_2 r)dr\right), \quad (16)$$

where Δ_1 and Δ_2 are combinations of the variances of the elastic moduli,

$$\Delta_1 = \frac{\alpha^2 M}{2P_d}\left(\sigma_{HH}^2 - 2\sigma_{HC}^2 + \sigma_{CC}^2 + \frac{32}{15}\frac{G^2}{H^2}\sigma_{GG}^2 - \frac{8}{3}\frac{G}{H}\sigma_{HG}^2 + \frac{8}{3}\frac{G}{H}\sigma_{GC}^2\right) \quad (17)$$

$$\Delta_2 = \Delta_1 + \frac{1}{2}\sigma_{HH}^2 - \frac{4}{3}\frac{G}{H}\sigma_{HG}^2 + \left(\frac{4G}{H} + 1\right)\frac{4}{15}\frac{G}{H}\sigma_{GG}^2. \quad (18)$$

Here we use $C = \alpha M$. In equation 16, $k_1 = \omega/c_P$ is the wavenumber of a P-wave in the homogeneous background medium with $c_P = \sqrt{H/\rho}$ and composite density $\rho = (1 - \phi)\rho_g + \phi\rho_f$; ρ_g and ρ_f are the densities of the grain material and fluid, respectively. Attenuation and dispersion are obtained from equation 16 in the usual way (White, 1983): $Q^{-1} = 2\Im\{\bar{k}_p\}/\Re\{\bar{k}_p\}$ and $v_P = \omega/\Re\{\bar{k}_p\}$. Equation 16, which is based on the first-order smoothing approximation, accounts for fluctuations in the poroelastic moduli H, G, and C but does not account for permeability fluctuations. An extended first-order approximation can be obtained by replacing the background, slow P-wavenumber k_2 (in equation 16) by its first-order approximation k_2^*, which is given by equation 3. The resulting P-wavenumber depends on the second-order statistics of all poroelastic parameters, including that of the permeability. Thus, the searched-for dependence of the fast P-wave characteristics on the permeability fluctuations is obtained. Note, as a result of the existence of a positive imaginary part in the expression for k_2^*, the resulting integrals converge for all correlation functions (that decrease with increasing argument).

Let us examine the validity range of the extended first-order approximation, i.e., the replacement of k_2 by k_2^* in equation 16 as proposed in the previous paragraph. The overall range of validity depends on the ranges of validity of the effective wavenumbers, k_1^* and k_2^*. As usual in perturbation theory, the results are assumed to be precise, provided that the additional terms coming from perturbation analysis (e.g., the second and third term on the right-hand side of equation 16) provide only a small correction to the background value. Applying this rule to the effective slow P-wavenumber (equation 3), we obtain the condition,

$$|\Delta_S \xi(\omega)| \ll 1. \quad (19)$$

The absolute value of the frequency-dependent function $\xi(\omega)$ assumes values between 0 and 1, so that the range of validity of k_2^* can be estimated as

$$\Delta_S \ll 1. \quad (20)$$

A similar analysis yields the applicability range for the first-order statistical smoothing approximation of k_1^* (see also equation 58 in Müller and Gurevich, 2005a):

$$\max\{\Delta_1(|k_2|a)^2, \Delta_2\} \ll 1. \quad (21)$$

The correction term for the extended first-order approximation is

$$\delta = \Delta_2 + \Delta_1 k_2^{*2}\int_0^\infty rB(r)\exp(ik_2^* r)dr. \quad (22)$$

Using the upper bound of $\xi(\omega)$ and the fact that the correction term of k_2^* produces an additional exponentially decreasing multiplier in the integral in 22, we find

$$\delta \le \Delta_2 + \Delta_1 k_2^2(1 + \Delta_S)\int_0^\infty rB(r)\exp(ik_2 r)dr$$
$$= \Delta_2 + \Delta_1 k_2^2 \int_0^\infty rB(r)\exp(ik_2 r)dr + O(\Delta^2). \quad (23)$$

Apart from terms of the order of $O(\Delta^2)$, i.e., terms containing the product $\Delta_1\Delta_S$, the last line corresponds to the correction term of the effective fast P-wavenumber which results into the applicability condition 21. To make our results consistent with the precision of the first-order statistical smoothing approximation, i.e., $O(\Delta)$, terms of the order of $O(\Delta^2)$ are neglected. We note that the smallness of the correction term δ is also fulfilled if the condition 20 is relaxed, whereby $\Delta_S \le 1$. In conclusion, the combined model is applicable if the conditions for the applicability of k_1^* and k_2^* are fulfilled (relations 20 and 21).

Figure 2 shows the reciprocal quality factor obtained from equation 16 by using the poroelastic parameters of Table 1 and by using $\Delta_1 = 0.060$, $a = 0.15$ m. If the constant background permeability value of $\kappa_0 = 250$ mD is used, we obtain the dashed curve. Using equation 16 in conjunction with the effective slow P-wavenumber given by equation 3, we obtain the solid curves (here we use $\Delta_S = 0.5$) for different correlation lengths of the permeability fluctuations a_p (ranging from $0.01a$ to $10a$; values of a_p outside this range do not produce an additional change in the attenuation behavior). For the case in which $a = a_p$, i.e., when correlation lengths of the

elastic moduli and permeability fluctuations coincide (this is a realistic assumption), three effects can be observed. First, the maximum seismic attenuation shifts to lower frequencies if we account for the permeability fluctuations (compared to the constant-background-permeability case). Second, the magnitude of attenuation is slightly reduced. Third, incorporation of the permeability fluctuations in equation 16 results in a broadening of the attenuation peak. At high frequencies, the permeability fluctuations have no impact and the attenuation is identical to that produced using the constant permeability model (circles). This is because the effective permeability model employed predicts that, at high frequencies, $\kappa^* = \kappa_0$. The phase velocity dispersion for the same model parameters (and for $\Delta_2 = 0.064$) is shown in Figure 3. Interestingly, the presence of permeability fluctuations increases the phase velocity (again, when compared with the constant-background-permeability case).

Strong permeability fluctuations in 1D random media

While the replacement $k_2 \Rightarrow k_2^*$ based on equation 3 is only valid for the weak fluctuation case, the implications of strong permeability fluctuations in 1D random media can be modeled by using an effective slow P-wavenumber involving the effective permeability (equation 14). We recall that equation 14 is obtained by rescaling the dispersion relation 3 such that the exact bounds at low and high frequencies are met. The strength of the permeability fluctuations is expressed through equation 15, which contains the ratio of harmonic and arithmetic average of the permeability fluctuations:

$$r = \left\langle \frac{1}{\kappa} \right\rangle^{-1} \langle \kappa \rangle^{-1} \equiv \frac{\bar{\kappa}_H}{\bar{\kappa}_A}. \tag{24}$$

That is, irrespective of the permeability contrast between individual layers, the overall contrast is controlled by the two end-members, $\bar{\kappa}_A$ and $\bar{\kappa}_H$. Obviously, this rescaled permeability model is incomplete in the sense that the rescaling introduces an arbitrary, large frequency shift of the whole dispersion curve (i.e., its shape is preserved but the location relative to the frequency axis is incorrect). This problem can be overcome when connecting the model with the results for the effective fast P-wavenumber: If there are no permeability fluctuations, it is known that maximum attenuation occurs at $\omega_{\max} = \kappa_0 N/(2a^2\eta) = D_0/a^2$, where D_0 is the diffusivity. This frequency is determined by either direct calculation or by computing the intersection point of the low- and high-frequency asymptotes of attenuation (Müller and Rothert, 2006). Assuming that the low-frequency asymptote of attenuation depends on $\bar{\kappa}_H$, whereas the high-frequency asymptote depends on $\bar{\kappa}_A$, the intersection point of these asymptotes yields the maximum frequency

$$\omega_{\max} = \frac{\sqrt{D_H D_A}}{a^2} = \frac{D_A\sqrt{r}}{a^2}, \tag{25}$$

where D_A and D_H denote the diffusivities involving $\bar{\kappa}_A$ and $\bar{\kappa}_H$, respectively. We use this frequency to fix the peak attenuation in the combined model. Hence, substituting $k_2^* = \sqrt{i\omega\eta/\kappa^{*(1D)}N}$ (with $\kappa^{*(1D)}$ as defined in equation 14) into the 1D version of equation 16 (see equation 56 in Gurevich and Lopatnikov, 1995), yields a new effec-

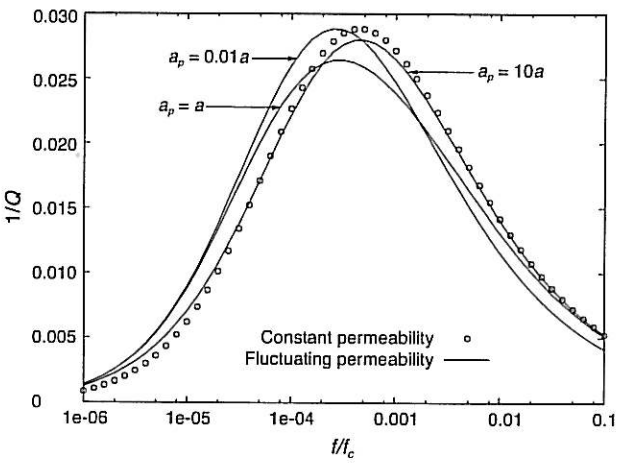

Figure 2. Frequency dependence of the inverse quality factor computed using equation 16. If there are no permeability fluctuations, one obtains the curve displayed with circles. In the case of permeability fluctuations, the solid curves are valid. Three regimes can be observed depending on the relation between the correlation lengths of the permeability fluctuations (a_p) and the poroelastic moduli fluctuations (a). If $a_p \approx a$, we can see that attenuation peaks at lower frequencies (with a slightly decreased magnitude) and that the curve becomes more broadened.

Table 1. Typical poroelastic parameters for a water-saturated, well-consolidated porous sandstone.

K_g	40 GPa
K_d	4.5 GPa
G	9 GPa
ϕ	0.17
κ_0	250 mD
ρ_g	2650 kg/m^3
K_f	2.17 GPa
η	0.001 Pa.s
ρ_f	1000 kg/m^3

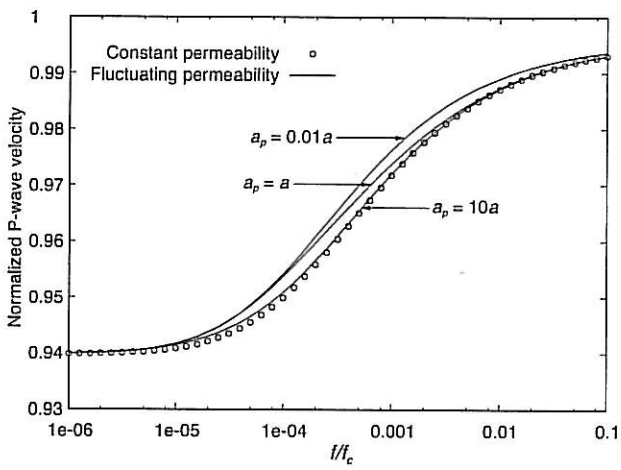

Figure 3. Frequency dependence of P-wave velocity (normalized to background velocity). The velocity-dispersion behavior for the constant permeability case is indicated by the circles. If permeability fluctuations are accounted for, one obtains from equation 16 the solid curves. As in Figure 2, the dependence of the dispersion on the relation between a and a_p is displayed. Note that in all cases, the presence of permeability fluctuations increases the phase velocity.

tive fast P-wavenumber $k_1^{*(1D)}$. The applicability range of this approximation is defined by relation 21. However, there is no restriction with respect to the strength of permeability fluctuations.

Figure 4 illustrates the resulting attenuation for a varying ratio of harmonic to arithmetic permeability using the parameters given in Table 1 as background a medium that is superimposed by random fluctuations with $\Delta_1 = 0.075$, $\Delta_2 = 0.081$, and $a = a_\kappa = 0.1$ m. The circles and squares denote the attenuation using the arithmetic- and harmonic-averaged permeability (with $r = 10^{-4}$), respectively. All effects observed in Figure 2 (weak-fluctuation case) can now be observed in an amplified manner. For $r = 10^{-4}$, the peak attenuation is shifted by factor $\sqrt{1/r} = 100$ and the magnitude is reduced by 30%. At very low frequencies, the attenuation behavior is controlled by the harmonic average of the permeability. Figure 5 displays the corresponding phase velocity dispersion. It can be observed that now the inflection point is shifted by the factor $\sqrt{1/r} = 100$.

The combination of the approximations for the fast and slow P-waves in random poroelastic media yields seismic attenuation and dispersion estimates that also depend on the statistical characteristics of the fluid transport properties. In the next section we see if the effects predicted theoretically can be confirmed with the help of numerical simulations.

NUMERICAL SIMULATIONS IN RANDOMLY LAYERED MEDIA

To validate the analytical model developed above, realizations of randomly layered media are created and wave propagation simulations are conducted using the OASES reflectivity code for poroelastic media (Stern et al., 1985; Schmidt and Tango, 1986). The OASES code allows numerical models to be constructed for horizontally stratified poroelastic layers by computing the plane wave, complex transmission coefficient T along with the associated phase. This coefficient can then be used to calculate the phase velocity V_p and attenuation $1/Q$ in an equivalent homogeneous medium. For normal incidence, the transmission coefficient T for such an equivalent medium can be written as

$$T = \exp(iKL) = \exp(-\gamma L)\exp(i\omega L/V_P), \qquad (26)$$

where L is the overall thickness of the layered system, $K = \omega/V_P + i\gamma$ is the complex wavenumber of the transmitted fast P-wave, and γ is the effective attenuation coefficient. Taking absolute values of the left- and right-hand sides of equation 26 yields

$$|T| = \exp(-\gamma L), \qquad (27)$$

or $\gamma = -\ln|T|/L$. Effective attenuation coefficient γ for low-loss media is related to the inverse quality factor $1/Q$ by (White, 1983)

$$Q^{-1} = \frac{2\gamma V_P}{\omega} = -\frac{2V_P}{L\omega}\ln|T|. \qquad (28)$$

Equation 28 is used to compute the inverse quality factor from absolute values of the transmission coefficients.

To construct random sequences of layers, we use a random number generator in conjunction with an autoregressive filter, which creates spatially correlated random numbers for fluid bulk modulus K_f and permeability κ (see also Shapiro and Müller, 1999). Altogether, an ensemble of 10 realizations to 200 layers with constant layer-thickness of 0.75 m are created. We note that fluctuations of any of the bulk moduli (and the shear modulus) produce wave-induced flow and that the choice of K_f-fluctuations only is to keep the numerical model simple. The ensemble is characterized by the spatial, normalized autocorrelation function:

$$\frac{\left\langle\left[K_f(z) - \bar{K}_f\right]\left[K_f(z-\varsigma) - \bar{K}_f\right]\right\rangle}{\bar{K}_f^2} = \sigma_{K_f}^2 \exp(-|\varsigma|/a), \qquad (29)$$

with a constant background value of $\bar{K}_f = 2.25$ GPa, correlation length $a_{K_f} = 1.43$ m, and standard deviation $\sigma_{K_f} = 0.22$, so that $\Delta_1 = 0.0013$. To obtain a positive permeability sequence, we randomized the logarithm of the permeability $s = \log(\kappa)$ using the normalized autocorrelation function,

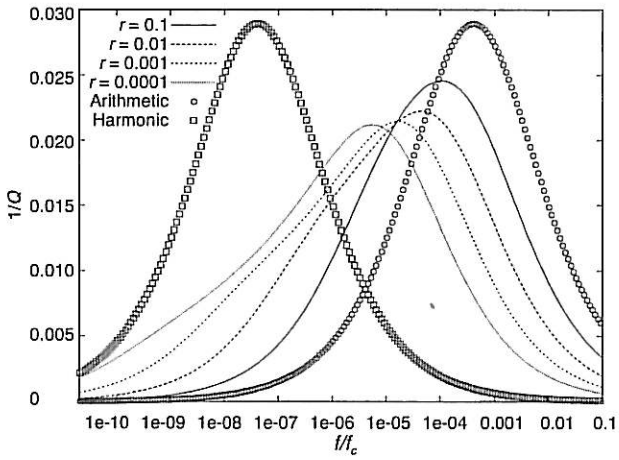

Figure 4. Frequency dependence of the inverse quality factor using the strong-contrast model involving equation 14. The ratio of harmonic to arithmetic average is denoted as r. With decreasing r, the peak attenuation shifts towards lower frequencies and its magnitude is smaller than that obtained for constant-permeability, random media involving the arithmetic/harmonic average of the permeabilities (circles and squares).

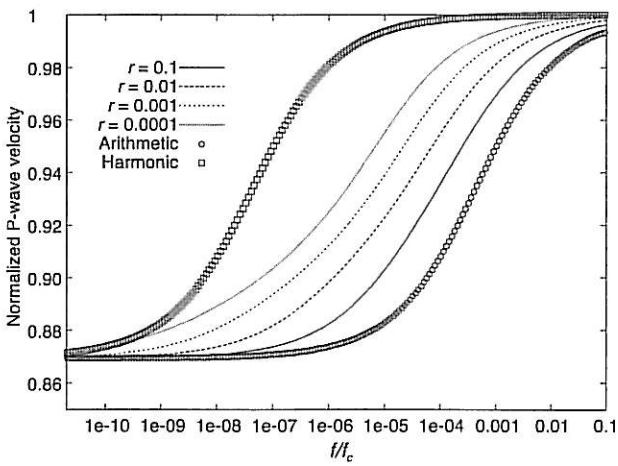

Figure 5. Frequency dependence of phase velocity for the same model as in Figure 4. Note the increase/decrease in phase velocity in the presence of permeability fluctuations compared to the velocity in random media involving the arithmetic/harmonic average of the permeabilities (circles and squares).

$$\frac{\langle [s(z) - \bar{s}][s(z - \varsigma) - \bar{s}] \rangle}{\bar{s}^2} = \sigma_s^2 \exp(- |\varsigma|/a), \quad (30)$$

with the constant correlation length $a_\kappa = 1.43$ m and such parameters $\bar{s}$ and σ_s that give for the ensemble an arithmetic average of $\bar{\kappa}_A = 8.15 \cdot 10^{-13}$ m^2 and a harmonic average of $\bar{\kappa}_H = 0.09 \cdot 10^{-13}$ m^2 ($r = 0.011$). The constant background medium is characterized by a porosity $\phi = 0.09$ and fluid viscosity $\eta = 5 \cdot 10^{-5}$ Pa.s (all other parameters are those of Table 1).

We construct three different models with the same fluctuations of the fluid bulk modulus but with different permeability values. Model I has random permeability values as specified above. In model II, the permeability is kept constant and equals the harmonic average $\bar{\kappa}_H$. Model III has a constant permeability for all layers that is equal to the arithmetic average $\bar{\kappa}_A$. The resulting P-wave attenuation as a function of frequency for these three models is displayed in Figure 6 (solid, dashed, and dotted line). The theoretical predictions for models II and III are computed using equation 16 whereby the slow P-wavenumber (equation 6) involves the harmonic and arithmetic average permeability values, respectively (squares and triangles). The theoretical prediction for model I is also computed using equation 16; however, it involves the effective slow wavenumber (equation 3) (depicted by circles). For all models, the attenuation of both the theoretical and numerical results matches reasonably well in magnitude and frequency dependence. Peak attenuation is almost identical for models II and III. There is approximately two orders of magnitude separation in the frequency at which maximum attenuation occurs for these two models. Both the numerical and theoretical attenuation peaks for model I are approximately 30% lower than the corresponding peaks for models II and III, whereas the peak frequency for model I is roughly between the peak frequencies for models II and III. At low and high frequencies, fluctuations of the numerical results can be observed. We verified that to increase the number of medium realizations does not lead to a further reduction of these fluctuations. They can be explained as follows. At high frequencies (say >20 Hz) we expect the contribution of scattering attenuation. This attenuation mechanism is not sensitive to permeability fluctuations, which explains the similarity of the modulations of all three numerical models. At low frequencies (say<0.7 Hz), the numerical values fluctuate around the theoretical curves with an increasing magnitude of fluctuations for decreasing frequencies (again showing similar modulations for all three models). These fluctuations are caused by resonance effects of the whole stack of layers which is sandwiched between two constant elastic half-spaces. They can be reduced by suitable choice of the elastic properties of the half-spaces and by the overall thickness of the stack of layers. Another difficulty is that, in the numerical model, the fluctuations of permeability are log-normally distributed, whereas theory assumes normally distributed random variables.

The numerical simulations indicate that the effects of permeability fluctuations on seismic attenuation in randomly layered media can be described by the theoretical approach developed above. In particular, the frequency shift of the attenuation behavior in the presence of permeability fluctuations is well predicted by the theoretical model.

DISCUSSION

From perturbation analysis, we find an expression for the effective Biot slow wavenumber from which we deduce a dynamic-equivalent permeability for 1D and 3D random porous media. This permeability is bounded by the arithmetic and harmonic averages of the permeabilities of the inhomogeneities:

$$\left\langle \frac{1}{\kappa} \right\rangle^{-1} = \bar{\kappa}^{(1D)}(\omega = 0)$$
$$< \bar{\kappa}^{(3D)}(\omega = 0) < \bar{\kappa}^{(1D,3D)}(\omega \to \infty) = \langle \kappa \rangle. \quad (31)$$

The proposed dynamic-equivalent permeability produces a negative scale effect (decreasing permeability for increasing observation scale). The expression for the dynamic-equivalent permeability is nonlocal and involves an integral over the spatial correlation fubnction of the permeability fluctuations.

The frequency-dependence of the permeability can be explained as follows. At low frequencies, the diffusion wavelength $\lambda = 2\pi/k_0$ is larger than the correlation scale of the fluctuations, and, therefore, fluid flow takes place on a spatial scale that encompasses many inhomogeneities. On average, these permeability fluctuations hinder the pressure equilibration (and hence the flow), so that the effective permeability is decreased (with respect to the background permeability). In 1D inhomogeneous media, the low-frequency limit of the permeability is given by the harmonic average, $\langle 1/\kappa \rangle^{-1}$. In 3D inhomogeneous media, the effect of permeability fluctuations on the effective permeability is less pronounced (because of the existence of high-permeability paths). At higher frequencies, i.e., if $\lambda \leq a$, fluid flow takes place on a spatial scale comparable to or smaller than the correlation length. This implies that only the local permeability value is relevant, which, upon ensemble averaging, yields the effective permeability, $\bar{\kappa} = \langle \kappa \rangle$. We note that the positive scale effect reported from field measurements is probably caused by preferred high-conductivity paths encountered as larger regions of the medium are analyzed. It is clear that the present theory, based on ensemble-averaged quantities (in a statistically homogeneous medium), does not account for such effects.

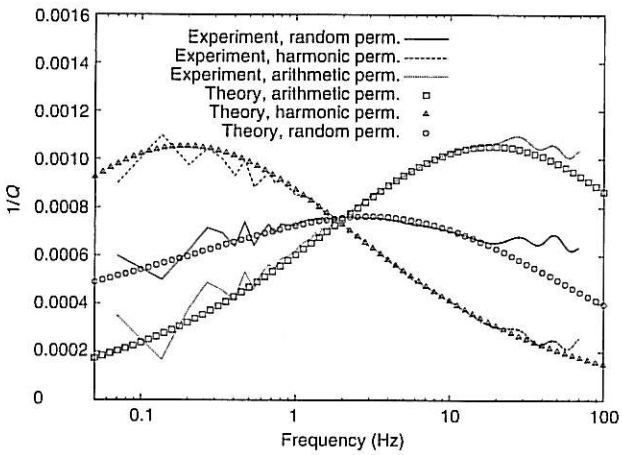

Figure 6. Attenuation as a function of frequency according to numerical simulations in randomly layered media including permeability fluctuations (solid line) and with constant permeability corresponding to the arithmetic and harmonic average of the permeability fluctuations (dotted and dashed lines). The corresponding theoretical predictions are also displayed (open symbols).

To examine the effect of permeability fluctuations on seismic signatures, we incorporate this dynamic-equivalent permeability model into expressions for seismic wave attenuation and dispersion related to wave-induced fluid flow. The most prominent feature of the resulting model is a frequency shift of the seismic attenuation that depends on the strength of the permeability fluctuations. For 1D random media it is possible to infer the impact of strong permeability fluctuations. Because the low- and high-frequency values of permeability coincide with the exact bounds regardless of the strength of fluctuations, we rescale the effective permeability model to these bounds (equation 14). Incorporating this rescaled model into the expressions for wave attenuation, we observe a significant frequency shift (Figures 4 and 5). Numerical simulations in stacks of randomly layered, poroelastic media confirm this picture. Extensions of the theory in order to model strong, log-normally distributed permeability variations in all space dimensions and including a permeability-porosity correlation are currently under investigation.

CONCLUSIONS

In conclusion, the results indicate that permeability fluctuations on the mesoscopic scale (of the order of several centimeters) affect seismic wave propagation. In particular, we have shown that seismic attenuation related to wave-induced flow can be observed in a broader frequency range in structures with nonuniform permeabilities than that in structures with uniform permeabilities. Given that the present results are based on perturbation analysis and, thus, allow only for relatively small fluctuations of the permeability, we hypothesize that for realistic permeability fluctuations, these effects are more pronounced. This hypothesis is supported by theoretical and numerical results for 1D random media. This means that the effect of wave-induced fluid flow can be observed in a broader frequency range than previously thought. And more importantly, any attempt to infer fluid transport properties from seismic attenuation measurements will fail if the permeability fluctuations are not properly accounted for.

ACKNOWLEDGMENTS

The authors thank the Deutsche Forschungsgemeinschaft (contract MU 1725/1-3), the Curtin Reservoir Geophysics Consortium, the Petroleum Exploration Society of Australia, and the ASEG for their support with this project.

APPENDIX A

MATHEMATICAL CONSIDERATIONS

Here we give a short derivation of the dispersion relation for Biot's slow wave in randomly heterogeneous porous media (equation 3). The derivation is analogous to that of the fast P-wavenumber given in great detail by Müller and Gurevich (2005a). Using a Green's-function approach to solve Biot's equations of dynamic poroelasticity in randomly inhomogeneous media, the averaged (mean) Green's function $\bar{\mathbf{G}}$ can be expressed by the following integral equation:

$$\bar{\mathbf{G}} = \mathbf{G}_0 + \int\int \mathbf{G}_0\mathbf{Q}\bar{\mathbf{G}}, \qquad \text{(A-1)}$$

where $\mathbf{G}_0$ denotes the matrix of Green tensors for an isotropic, poroelastic whole-space in which only slow P-wave interactions are accounted for (that means that no coupling with the fast wave modes is possible):

$$\mathbf{G}_0 = \frac{\kappa_0}{4\pi i\omega}\partial_i\partial_j\frac{\exp(ik_2R)}{R}\begin{bmatrix} -\dfrac{C^2}{H^2} & \dfrac{C}{H} \\ \dfrac{C}{H} & -1 \end{bmatrix}. \qquad \text{(A-2)}$$

Here R is the source-receiver distance, and partial spatial derivatives are denoted as ∂_i. $\mathbf{Q}$ is the matrix of the so-called kernel-of-mass operators,

$$\mathbf{Q} = \left\langle \tilde{\mathbf{L}}\mathbf{G}_0\tilde{\mathbf{L}} + \int \tilde{\mathbf{L}}\mathbf{G}_0\tilde{\mathbf{L}}\mathbf{G}_0\tilde{\mathbf{L}} + \int \cdots \right\rangle, \qquad \text{(A-3)}$$

containing linear combinations of all even statistical moments of the random fields. The fluctuations of the random fields X [defined via $X = \bar{X}(1 + \varepsilon_X) = \bar{X}(1 + \tilde{X}/\bar{X})$, where the mean value is $\langle X\rangle = \bar{X}$] of the poroelastic parameters H, M, and $C = \alpha M$ are collected in the perturbation operator matrix

$$\tilde{\mathbf{L}} = \begin{bmatrix} \partial_i\tilde{H}\partial_j & \partial_i\tilde{C}\partial_j \\ \partial_i\tilde{C}\partial_j & i\omega\bar{\rho}\delta_{ij} + \partial_i\tilde{M}\partial_j \end{bmatrix}. \qquad \text{(A-4)}$$

Equation A-1 for the matrix of mean Green's tensors is too complicated to be solved exactly. Instead, one or another approximation must be employed. The method of statistical smoothing consists of truncating $\mathbf{Q}$ after the first term:

$$\mathbf{Q}^B \approx \left\langle \tilde{\mathbf{L}}\mathbf{G}_0\tilde{\mathbf{L}} \right\rangle. \qquad \text{(A-5)}$$

This truncation implies that the range of validity is restricted by small fluctuations. By means of the spatial Fourier transform,

$$G(\mathbf{r} - \mathbf{r}') = \int g(\mathbf{K})\exp(i\mathbf{K}\cdot(\mathbf{r} - \mathbf{r}'))d\mathbf{K} \qquad \text{(A-6)}$$

$$g(\mathbf{K}) = \frac{1}{(2\pi)^3}\int G(\mathbf{r} - \mathbf{r}') \times\exp(-i\mathbf{K}\cdot(\mathbf{r} - \mathbf{r}'))d(\mathbf{r} - \mathbf{r}'), \qquad \text{(A-7)}$$

the [2,2] component of the mean Green's tensor matrix (equation A-1) becomes

$$\bar{g} = g_0 + (8\pi^3)^2 g_0 q^B \bar{g}. \qquad \text{(A-8)}$$

Similar equations for the other tensor components can be obtained but are not needed in the sequel. In equation A-8, q^B denotes the spatial Fourier transform of the corresponding [2,2] component of $\mathbf{Q}^B$:

$$\mathbf{Q}^B_{[2,2]} = \left\langle \tilde{\mathbf{L}}_{[1,2]}\mathbf{G}_{[1,1]}\tilde{\mathbf{L}}_{[1,2]} \right\rangle + 2\left\langle \tilde{\mathbf{L}}_{[1,2]}\mathbf{G}_{[1,2]}\tilde{\mathbf{L}}_{[2,2]} \right\rangle + \left\langle \tilde{\mathbf{L}}_{[2,2]}\mathbf{G}_{[2,2]}\tilde{\mathbf{L}}_{[2,2]} \right\rangle, \qquad \text{(A-9)}$$

where $\tilde{\mathbf{L}}_{[x,y]}, \mathbf{G}_{[x,y]}$ are the [x,y] component of equations A-2 and A-4, respectively. If we assume that the mean Green's function $\bar{g}$ is of the same functional form as g_0 involving an effective wavenumber k^* instead of k_0, equation A-8 reduces to an algebraic equation for k^*:

$$k^{*2} \approx k_0^2\left[1 + \frac{8\pi^3\kappa_0}{i\omega}q^B\right]. \qquad \text{(A-10)}$$

That means that the only remaining problem is to evaluate the truncated kernel-of-mass operator matrix element Q^B and its spatial Fourier transform q^B. This computation is analogous to that in Müller and Gurevich (2005a, Appendix B) and involves the following steps. Using partial integrations, the spatial derivatives of the perturbation operators can be shifted to the Green's tensor. Averaging implies that $\langle\tilde{X}\tilde{Y}\rangle = B_{XY} = \sigma^2_{XY}B$ (where B is the normalized correlation function such that $B(0) = 1$) and yields, for each term on the right-hand side of equation A-9, expressions of the form

$$Q^{XY}_{ik} = \partial_i B_{XY} G_{jl,jl}\partial_k. \qquad \text{(A-11)}$$

Inverse Fourier transform of these expressions yields, then, $q^B = q^{MM} + q^{CM} + q^{CC} + q^{pp}$, which, after substitution into equation A-10, yields equation 3, with the frequency-dependent function ξ (equation 4). The corresponding 1D result (equations 7 and 8) can be derived from the 3D result using the Fresnel approximation as shown in Müller and Gurevich (2005a). The coefficients of the various q terms are collected in a single parameter Δ_S:

$$\Delta_S = \frac{C^4}{H^2N^2}\sigma^2_{CC} - \frac{C^2M}{HN^2}\sigma^2_{CM} + \frac{M^2}{N^2}\sigma^2_{MM} + \frac{\sigma^2_{pp}}{3}$$
$$= \frac{1}{P_d}\langle(\alpha^2M\varepsilon_C - H\varepsilon_M)^2\rangle + \frac{\sigma^2_{pp}}{3}. \qquad \text{(A-12)}$$

Using the relations between the relative fluctuations $\varepsilon_M = \varepsilon_{K_f} - \varepsilon_\phi$ and $\varepsilon_C = \varepsilon_\alpha - \varepsilon_M$ yields Δ_S as given by equation 5.

APPENDIX B

LIST OF SYMBOLS

κ_0, κ^* = Permeability, effective (dynamic-equivalent) permeability
$\Delta_S, \Delta_1, \Delta_2$ = Dimensionless coefficient composed out of linear combinations of the variances of the random fields
η = Fluid viscosity
ϕ = Porosity
α = Biot-Willis coefficient
ρ_g, ρ_f, ρ = Mass density of grain material, fluid phase, porous composite
G = Shear modulus of porous material
K_d, K_f, K_g = Bulk moduli of the solid phase, the drained frame, and the fluid phase
P_d, H = Drained and saturated P-wave modulus
M = Pore space modulus
N = Poroelastic modulus
k_2, k_2^* = Wavenumber of Biot's slow wave, dynamic-equivalent slow P-wavenumber
k_1, k_1^* = Fast P-wavenumber, dynamic-equivalent P-wavenumber
ε_X = Average-normalized fluctuations of random field X
$B(r)$ = Normalized correlation function
a_X = Correlation length associated with random field X
σ^2_{XY} = Normalized cross-variance of random fields X, Y
T = Complex transmission coefficient
L = Overall thickness of stack of layers
Q^{-1} = Inverse quality factor
γ = Attenuation coefficient

REFERENCES

Beran, M. J., 1968, Statistical continuum theories: John Wiley & Sons.

Bernabé, Y., C. Bruderer-Weng, and A. Maineult, 2003, Permeability fluctuations in heterogeneous networks with different dimensionality and topology: Journal of Geophysical Research, **108**, 2351.

Berryman, J. G., 1986, Elastic wave attenuation in rocks containing fluids: Applied Physics Letters, **49**, 552–554.

——, 1988, Seismic wave attenuation in fluid-saturated porous media: Pure and Applied Geophysics, **128**, 423–432.

Biot, M. A., 1956, Theory of propagation of elastic waves in a fluid-saturated porous solid, I. Low frequency range: Journal Acoustical Society America, **28**, 168–178.

——, 1962, Mechanics of deformation and acoustic propagation in porous media: Journal Applied Physics, **33**, 1482–1498.

Carcione, J. M., S. Picotti, S., 2006, P-wave attenuation by slow-wave diffusion: Effects of inhomogeneous rock properties: Geophysics, **71**, no. 3, O1–O8.

Gelinsky, S., and S. A. Shapiro, 1997, Dynamic-equivalent medium approach for thinly layered saturated sediments: Geophysical Journal International, **128**, F1–F4.

Gelinsky, S., S. A. Shapiro, T. Müller, and B. Gurevich, 1998, Dynamic poroelasticity of thinly layered structures: International Journal Solids Structures, **35**, 4739–4752.

Gurevich, B., and S. L. Lopatnikov, 1995, Velocity and attenuation of elastic waves in finely layered porous rocks: Geophysical Journal International, **121**, 933–947.

Gurevich, B., V. B. Zyrianov, and S. L. Lopatnikov, 1997, Seismic attenuation in finely layered porous rocks: Effects of fluid flow and scattering: Geophysics, **62**, 319–324.

Hristopulos, D. T., and G. Christakos, 1997, Variational calculation of the effective fluid permeability of heterogeneous media: Physical Review E, **55**, 7288–7298.

Johnson, D. L., J. Koplik, and R. Dashen, 1987, Theory of dynamic permeability and tortuosity in fluid-saturated porous media: Journal of Fluid Mechanics, **176**, 379–402.

Keller, J. B., 2001, Flow in random porous media: Transport in Porous Media, **43**, 395–406.

Müller, T. M., and B. Gurevich, 2005a, A first-order statistical smoothing approximation for the coherent wave field in random porous media: Journal Acoustical Society America, **117**, 1796–1805.

——, 2005b, Wave-induced fluid flow in random porous media: Attenuation and dispersion of elastic waves: Acoustical Society America, **117**, 2732–2741.

——, 2006, Effective hydraulic conductivity and diffusivity of randomly heterogeneous porous solids with compressible constituents: Applied Physics Letters, **88**, 121924.

Müller, T. M., and E. Rothert, 2006, Seismic attenuation due to wave-induced flow: Why Q scales differently in random structures: Geophysical Research Letters, **33**, L16305.

Pride, S. R., J. G. Berryman, and J. M. Harris, 2004, Seismic attenuation due to wave-induced flow: Journal of Geophysical Research, **109**, B01201.

Pride, S. R., E. Tromeur, and J. G. Berryman, 2002, Biot slow-wave effects in stratified rock: Geophysics, **67**, 271–281.

Pride, S. R., J. H. Harris, D. L. Johnson, A. Mateeva, K. T. Nihel, R. L. Nowack, J. W. Rector, H. Spetzler, R. Wu, T. Yamomoto, J. G. Berryman, and M. Fehler, 2003, Acquisition/processing — Permeability dependence of seismic amplitudes: The Leading Edge, **22**, 518–525.

Schmidt, H., and G. Tango, 1986, Efficient global matrix approach to the computation of synthetic seismograms: Geophysical Journal of the Royal Astronomical Society, **84**, 331–359.

Schulze-Makuch, D., D. A. Carlson, D. S. Cherkauer, and P. Malik, 1999, Scale dependency of hydraulic conductivity in heterogeneous media: Ground Water, **37**, 904–918.
Shapiro, S. A., and T. M. Müller, 1999, Seismic signatures of permeability in heterogenous porous media: Geophysics, **64**, 99–103.
Stern, M., A. Bedford, and H. R. Millwater, 1985, Wave reflection from a sediment layer with depth-dependent properties: Journal of the Acoustical Society America, **77**, 1781–1788.
White, J. E., 1983, Underground sound: Applications of seismic waves: Elsevier.